

Investigation of Proper Orthogonal Decomposition for Echo State Networks

Jean Panaioti Jordanou^a, Eric Aislan Antonelo^a, Eduardo Camponogara^a,
Eduardo Gildin^b

^a*Department of Automation and Systems, Federal University of Santa Catarina, R. Eng. Agrônomo Andrei Cristian Ferreira, s/n, Florianópolis, 88040-900, Santa Catarina, Brazil*

^b*Harold Vance Department of Petroleum Engineering, Texas A&M University, 3116 TAMU, 245 Spence St, College Station, TX 77843, Texas, United States of America*

Abstract

Echo State Networks (ESN) are a type of Recurrent Neural Networks that yields promising results in representing time series and nonlinear dynamic systems. Although they are equipped with a very efficient training procedure, Reservoir Computing strategies, such as the ESN, require the use of high order networks, i.e. large number of layers, resulting in number of states that is magnitudes higher than the number of model inputs and outputs. This not only makes the computation of a time step more costly, but also may pose robustness issues when applying ESNs to problems such as Model Predictive Control (MPC) and other optimal control problems. One such way to circumvent this is through Model Order Reduction strategies such as the Proper Orthogonal Decomposition (POD) and its variants (POD-DEIM), whereby we find an equivalent lower order representation to an already trained high dimension ESN. The objective of this work is to investigate and analyze the performance of POD methods in Echo State Networks, evaluating their effectiveness. To this end, we evaluate the Memory Capacity (MC) of the POD-reduced network in comparison to the original (full order) ENS. We also perform experiments on two different numerical case studies: a NARMA10 difference equation and an oil platform containing two wells and one riser. The results show that there is little loss of performance comparing the original ESN to a POD-reduced counterpart, and also that the performance of a POD-reduced ESN tend to be superior to a normal ESN of the same size. Also we attain speedups of around 80% in comparison to the original ESN.

Keywords: Model Order Reduction, Reservoir Computing, Echo State Networks.

1. Introduction

Recurrent Neural Networks (RNN) are very relevant in applications related to modeling real world phenomena when time-dependent data are available [1], [2], and are considered universal approximators of dynamic systems. As RNNs are nonlinear, their training suffers from issues such as local minima, slow training, and the so-called “fading gradient” problem [3], which is a numerical problem inherent in Backpropagation Through Time (BPTT) [4], the algorithm used to calculate an RNN gradient. While some solutions focus on solving the fading gradient problem by changing the RNN structure, such as the Long Short-Term Memory (LSTM) network [5], or the gated recurrent unit [3], another flavor of RNN is worthy of attention: Reservoir Computing (RC). RC simplifies the learning by dividing the RNN into two parts: a high-dimensional recurrent nonlinear layer, called reservoir, with fixed, randomly generated weights, and an adaptive readout output layer, which computes an instantaneous linear combination of the dynamic reservoir states [6]. The weights of the output layer are trained through linear least squares, overcoming the problems related to nonlinear training and BPTT. The term *Reservoir Computing* was actually established as an unifying framework for Liquid State Machines [7], and Echo State Networks (ESN) [6], both of which are methods for RNN training independently developed.

ESNs follow the general reasoning of Reservoir Computing: they adopt an architecture with a dynamic reservoir with fixed weights that projects the input to a high-dimensional space, and a trainable static readout output layer. The dynamic reservoir needs to have a large number of neurons [6], and the so-called Echo State property, which refers to stability properties of the network. There are many successful applications of ESNs, such as: learning complex goal-directed robot behaviors [8], fuel cell lifetime prediction [9], wind speed prediction [10], and medium voltage insulators classification [11]. Actually, the large number of dynamic states in the reservoir is a very important characteristic, as the output, being a linear combination of them, can represent a larger repertoire of dynamics. However, using ESNs as dynamic models for problems such as optimization and MPC (Model Predictive Control) [12] may be an issue since the higher the number of states in the ESN is, the larger is the optimization problem overall. This is because the number

of states in the ESN heavily dominates the number of inputs and outputs in the optimization problem, making it inherently larger and harder to solve.

As ESNs are high-dimensional, model order reduction methods may be used to find equivalent ESN models that have a considerably smaller number of states, but which still keeps the properties and performance of the original high-dimensional ESN. For that end, we count on Proper Orthogonal Decomposition (POD) [13], which applies Singular Value Decomposition (SVD) to find an optimal linear transformation that represents the state space of a large dynamical system in a more compact form. POD is already widely used to reduce the number of states of large dynamical models, specially phenomenological models such as a gas reservoir simulator [14] with tens of thousands of variables. Actually, POD has one disadvantage concerning nonlinear systems: although the method can in fact reduce the number of states, it does not reduce the computation number of nonlinear functions. There are developments of interpolation methods, such as the Discrete Empirical Interpolation Method (DEIM) [13], to mitigate the issue, by pivoting and approximating the nonlinear portion of the given model computation. Both POD and DEIM can be used to find lower-dimensional networks that are equivalent to the original ESN and, thus, have the potential to alleviate the computational burden of simulations that depend on the size of the trained ESN.

The main objective of this work is to experiment on the use of POD and DEIM for obtaining a reduced order equivalent for an already trained ESN. For such end, we apply the reduction given by POD in three different contexts: a Memory Capacity (MC) [15] evaluation experiment; a NARMA10 difference equation [16]; and a simulated oil platform containing two gas-lifted oil wells and one riser [17]. Additionally, we have shown results using DEIM-based reduction for the ESN on the first and last aforementioned experiments. We compare the performance of the reduced ESN to the original (non-reduced) ESN in the three experiments above, and also to another ESN of size equivalent to the reduced ESN's size in the MC and NARMA experiments.

In this context, our main contribution is the proposal and evaluation of Model Order Reduction (MOR) to reduce the number of states in an Echo State Network through several experiments. Furthermore, this work contributes by showing experimentally:

- that the memory capacity of a ESN reduced by POD is in general

higher than the memory capacity of a non-reduced ESN of equivalent size. This difference in memory capacity is greater as the desired ESN gets smaller in size.

- that, given two equally sized echo state networks, with the same number of reservoir’s states, the one obtained from POD reduction has a higher probability of generating a good enough reservoir for the considered task. This result is more evident and relevant as the size of the desired reservoir gets smaller.
- that, by employing a MOR method on ESNs, this work makes small ESNs more robust and performant, improving their suitability for real-time or embedded applications with memory limitations.
- that DEIM reduction alone for ESNs does not achieve satisfactory results in comparison to pure POD reductions.

This paper is organized as follows: Section 2 contains related works, Section 3 presents the Echo State Networks, Section 4 describes POD and DEIM, Section 5 reports on the case studies and experimental testing for the reduced ESN, and Section 7 concludes the work.

2. Related Work

There are works in the literature that address the issue of reducing the model size in reservoir computing. One of them is [16], where they propose reducing the number of states by considering the output as a linear combination of the states at different instants in time, comparing to an original ESN through the Information Processing Capacity (IPC) metric, and also applying the proposal to a NARMA system and the generalized Hénon-map. The solution raises the effective number of states as a multiple of the delay or “drift-state” number utilized. The architecture is very hardware-friendly, easing the computation in relation to a standard ESN. Another example is the work [18], where they propose to employ the controllability matrix of the ESN as a means to find a so-called minimal ESN, which would be the ESN with the smallest reservoir that could reproduce the task at hand. They train the ESN for a given task, obtain the controllability matrix at given points, and define its rank as a new candidate reservoir size. An extensive search procedure is then performed to find the optimal ESN at that given

size, however there is no direct connection between the larger and the smaller ESN. In summary, the method in [18] proposes an interesting way of finding a minimal reservoir for a task. In comparison, our work follows a different direction: reducing the size of the network through the Singular Value Decomposition (SVD). Another work [19] proposes a different approach on reducing reservoir size, by calculating the correlation between each neuron, and eliminating the reservoir neurons with highest correlation.

The necessary large number of reservoir state in an ESN implies a complex computational model, therefore works such as [20], employ methods of so-called “network size reduction,” by performing multi-objective optimization on the output weights, minimizing not only the least-square error, but also the number of non-zero elements in the output weights. Enforcing sparseness is ideal to make the ESN easier to compute. Another work that follows this line of reasoning is [21], where they enforce a minimum complexity ESN by forcing the ESN reservoir to follow a deterministic form (i.e., a circular reservoir).

In [22], they propose to add the reservoir dimensionality reduction into the architecture via Principal Component Analysis (PCA), and calculate the output layer based on the PCA output instead of the reservoir states. They affirm that this enhances the dynamic properties of the resulting ESN in relation to the system identified, and improves the network generalization capabilities. Also, that applying dimensionality reduction in the states renders the ESN a tool for dynamic system analysis. In this sense, our POD-ESN method is similar to PCA with respect to obtaining the new state space, but goes beyond [22] by embedding the reduction achieved in the reservoir’s state update equation. This is to say that the reservoir recurrent simulation is accomplished in the reduced state space with POD-ESN, which does not happen in [22].

Another interesting approach of reduction in reservoir computing, not involving POD, is proposed in [23]. Their idea involves procedurally removing neurons according to the output weight value, which they curiously discovered that the network performance improves (given the Lorentz system as application) when neurons associated with large output weights are removed. They thoroughly analyze the effect of removing different types of nodes in the ESN. The aforementioned method can reduce an ESN size up to 60% without compromising performance.

3. Echo State Networks (ESN)

An ESN is a type of recurrent neural network with useful characteristics for system identification [6], as it represents nonlinear dynamics well and the training consists in solving a linear least-squares problem of relatively low computational cost when compared to nonlinear optimization.

3.1. Model

Proposed in [24, 25], the ESN is governed by the following discrete-time dynamic equations:

$$\begin{aligned} \mathbf{x}[k+1] &= (1 - \gamma)\mathbf{x}[k] \\ &\quad + \gamma\mathbf{f}(\mathbf{W}_r^r\mathbf{x}[k] + \mathbf{W}_i^r\mathbf{u}[k] + \mathbf{W}_b^r + \mathbf{W}_o^r\mathbf{y}[k]) \end{aligned} \quad (1)$$

$$\mathbf{y}[k+1] = \mathbf{W}_r^o\mathbf{x}[k+1], \quad (2)$$

where: the state of the reservoir neurons at time k is given by $\mathbf{x}[k]$; the current values of the input and output neurons are represented by $\mathbf{u}[k]$ and $\mathbf{y}[k]$, respectively; γ is called leak rate [6], which governs the percentage of the current state $\mathbf{x}[k]$ that is transferred into the next state $\mathbf{x}[k+1]$. The weights are represented in the notation $\mathbf{W}_{\text{from}}^{\text{to}}$, with “b”, “o”, “r”, and “i” meaning the bias, output, reservoir, and input neurons, respectively; and $f = \tanh(\cdot)$ is an activation function widely used in the literature, also called a base function in system identification theory [1]. Fig. 1 depicts a standard architecture of an echo state network.

The network has N neurons in the reservoir, which is the dimension of $\mathbf{x}[k]$ and is typically orders of magnitude higher than the number of network inputs. As long as regularization is used in network training, N can be as large as needed, but at the expense of increased computation time to update the reservoir states as defined in (1). According to [15], the ESN with no output feedback connections (the output has no effect on the state), which is given by \mathbf{W}_o^r , has a memory capacity (MC) bounded by the number of neurons in the reservoir ($MC \leq N$), assuming that linear output units are used.

The recurrent reservoir should possess the so-called Echo State Property (ESP) [25], i.e., a fading memory of its previous inputs, meaning that influences from past inputs on the reservoir states vanish with time. The ESP is guaranteed for reservoirs with $\tanh(\cdot)$ as the activation function, provided that the singular values of $\mathbf{W}_r^r < 1$. However, this condition limits

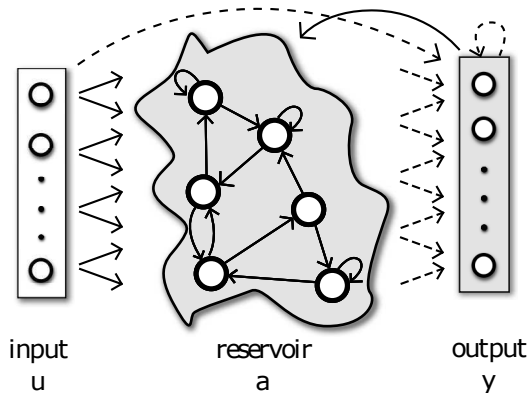


Figure 1: Representation of an Echo State Network, one of the possible models in Reservoir Computing. Dashed connections (from Reservoir to Output Layer) are trainable, while solid connections are fixed and randomly initialized.

the richness of the reservoir dynamical qualities, which discourages its use in practice. Note that all connections going to the reservoir are randomly initialized, usually according to the following steps:

1. Every weight of the network is initialized from a normal distribution $\mathcal{N}(0, 1)$.
2. \mathbf{W}_r^r is scaled so that its spectral radius ρ (Eigenvalue with the largest module) characterizes a regime able to create reservoirs with rich dynamical capabilities. It has been often observed that setting $\rho < 1$ in practice generates reservoirs with the ESP [6]. However, reservoirs with $\rho > 1$ can still have the ESP since the effective spectral radius may still be lower than 1 [26, 27].
3. \mathbf{W}_i^r and \mathbf{W}_b^r are multiplied by scaling factors f_i^r and f_b^r , respectively, affecting the magnitude of the input.

These scaling parameters, ρ , f_i^r , and f_b^r are crucial in the learning performance of the network, having an impact on the nonlinear representation and memory capacity of the reservoir [28]. Also, low leak rates allow for higher memory capacity in reservoirs, while high leak rates should be favored for quickly varying inputs and/or outputs. The settings of these parameters should be such that the generalization performance of the network (loss on a validation set) is enhanced.

3.2. Training

While in standard RNNs all weights are trained iteratively using gradient descent [4], ESNs restrict the training to the output layer \mathbf{W}_r^o . Because the echo state property is not insured with output feedback $\mathbf{W}_o^r \mathbf{y}[k]$, this work favors reservoirs without feedback from the output (i.e., $\mathbf{W}_o^r = 0$). Also, the inputs do not interfere directly in the output, as systems with direct transmission are less smooth and more sensitive to noise. To train an ESN, the input data $\mathbf{u}[k]$ is arranged in a matrix \mathbf{U} and the desired output $\mathbf{d}[k]$ in vector \mathbf{D} over a simulation time period, where each row \mathbf{u}^T of \mathbf{U} corresponds to a sample time k and its columns are related to the input units. For the sake of simplicity, we assume that there are multiple inputs and only one output. The rows of \mathbf{U} are input into the network reservoir according to each sample time, thereby creating a state matrix \mathbf{X} that contains the resulting sequence of states. Then, we apply the Ridge Regression algorithm [2] by using \mathbf{X} as the input data matrix and \mathbf{D} as the output data matrix, or in this case a vector as we assumed single output. Ridge Regression results in solving the following linear system:

$$(\mathbf{X}^T \mathbf{X} - \lambda \mathbf{I}) \mathbf{W}_r^o = \mathbf{X}^T \mathbf{D}, \quad (3)$$

where λ is the Tikhonov regularization parameter, which serves to penalize the weight magnitude, and avoid overfitting. There are also methods to apply least squares training in an online way [1], but these algorithms are not used in this work.

4. Model Order Reduction

In this section, we propose Model Order Reduction (MOR) methods for reducing the reservoir dimensionality in ESNs. Specifically, the Proper Orthogonal Decomposition (POD) and the Discrete Empirical Interpolation Method (DEIM) are presented. We also propose a strategy for correcting the steady-state error introduced in ESNs by MOR methods.

4.1. Proper Orthogonal Decomposition

The Proper Orthogonal Decomposition is a method to find a linear transformation [29] \mathbf{T} for a given system that maps a high-dimensional state space into a reduced one, namely:

$$\mathbf{x} = \mathbf{T} \mathbf{z} \quad (4)$$

where \mathbf{x} is a vector of dimension n and \mathbf{z} is a vector of dimension $m \ll n$, so that $\mathbf{T} \in \mathbb{R}^{n \times m}$.

The transformation itself is akin to a similarity transformation, with the main difference being that \mathbf{T} lacks an inverse for not being a square matrix. However, the \mathbf{T} resulting from POD is orthonormal ($\mathbf{T}^T \mathbf{T} = \mathbf{I}$), so the transpose is used in place of an inverse.

To find \mathbf{T} , we gather snapshots of the states in a given dynamical system response, akin to gathering data in a machine learning problem. The columns of the snapshot matrix $\mathbf{X} \in \mathbb{R}^{n \times N}$ are the states $\mathbf{x}[k] \in \mathbb{R}^n$, where N is the number of snapshots such that $N \geq n$. Then, we wish to minimize the error induced by projecting the original state onto the reduced space and back, which leads to the following error function:

$$E(\mathbf{T}) = \sum_{k=1}^N (\mathbf{x}[k] - \underbrace{\mathbf{T} \mathbf{T}^T \mathbf{x}[k]}_{\mathbf{z}[k]})^2 \quad (5)$$

The second term is \mathbf{x} *projected* onto the reduced space of \mathbf{z} , and then *lifted* back. The optimal \mathbf{T} is obtained through singular value decomposition (SVD) [30], decomposing \mathbf{X} in the following form:

$$\mathbf{U}_{\text{svd}} \mathbf{\Sigma} \mathbf{V}^T = \mathbf{X} \quad (6)$$

where \mathbf{U}_{svd} contains the left singular vectors and has dimension $n \times n$, $\mathbf{\Sigma}$ contains the singular values and has dimension $n \times N$, with only n non-zero columns. We consider that $\mathbf{\Sigma}$ is sorted from the largest to the smallest singular value. The right singular vector matrix \mathbf{V} is not used for POD.

The transformation \mathbf{T} that minimizes $E(\mathbf{T})$ is found by concatenating the columns with the m largest corresponding singular values from \mathbf{U}_{svd} . We seek a truncation so that the reduced system energy is close to the original, measured by:

$$\epsilon = \sum_{j=1}^m \epsilon_j \quad \epsilon_j = \sigma_j / \sum_{i=1}^n \sigma_i \quad (7)$$

where ϵ is the total energy contribution of the singular values maintained in the reduced-order model, σ_j is the j^{th} highest singular value, ϵ_j is the energy contribution of that given singular value, and m is the reduced state dimension. For this work, we measure the energy contribution of each singular

value of the original signal, and truncate \mathbf{U}_{svd} to obtain \mathbf{T} so that ϵ reaches a desired energy contribution value (*e.g.*, $\epsilon = 0.95$ so that the reduced system has 95% of the original system's energy). After obtaining \mathbf{T} for the dimension reduction through the process above, the reduced ESN dynamics can be expressed as follows:

$$\begin{aligned} \mathbf{z}[k+1] &= (1-\gamma)\mathbf{z}[k] \\ &\quad + \gamma\mathbf{T}^T\mathbf{f}(\mathbf{W}_r^r\mathbf{T}\mathbf{z}[k] + \mathbf{W}_i^r\mathbf{u}[k] + \mathbf{W}_b^r) \end{aligned} \quad (8a)$$

$$\mathbf{y}[k+1] = \mathbf{W}_r^o\mathbf{T}\mathbf{z}[k+1], \quad (8b)$$

It can be observed from the operation $\mathbf{T}^T\mathbf{f}(\cdot)$ that the reduced-order ESN does not actually reduce the number of computations by only performing POD on it. In fact, to compute the element-wise \tanh , \mathbf{T} brings the dimension back to the original state space size, which is to be reduced again with \mathbf{T}^T , increasing the number of computations in the end. This computational increase is inherent in POD for nonlinear systems and will be dealt with by the method described in the next section.

4.2. Discrete Empirical Interpolation

The Discrete Empirical Interpolation Method (DEIM) is an approximation method to circumvent the POD computation issue [13], which consists of state projection and lifting operations to compute state transitions in the reduced-order model. The core idea of DEIM is to approximate the nonlinear term of a dynamic system as a polynomial interpolation that resembles the strategy employed in POD. Given the following discrete-time nonlinear system:

$$\mathbf{x}[k+1] = \mathbf{A}\mathbf{x} + \mathbf{f}(\mathbf{x}[k]), \quad (9)$$

where the nonlinear function is elementwise, meaning that $\mathbf{f} = (f(\mathbf{x}), f(\mathbf{x}), \dots, f(\mathbf{x}))$ for a given function f such as \tanh . Notice that the system is divided into a linear and nonlinear portion. Applying the POD ($\mathbf{x} = \mathbf{T}\mathbf{z}$) into such a system yields:

$$\mathbf{z}[k+1] = \mathbf{T}^T\mathbf{A}\mathbf{T}\mathbf{z}[k] + \mathbf{T}^T\mathbf{f}(\mathbf{T}\mathbf{z}[k]) \quad (10)$$

The nonlinear mapping \mathbf{f} of the dynamic system can be approximated as follows:

$$\mathbf{P}^T\mathbf{f}(\mathbf{T}\mathbf{z}[k]) \approx \mathbf{P}^T\mathbf{U}\mathbf{c}[k] \quad (11)$$

where $\mathbf{U} \in \mathbb{R}^{n \times m}$, which is obtained from the same POD as \mathbf{T} , however with a different number m of singular vectors, with n being the number of states,

and \mathbf{P} is a pivoting matrix of the same dimension as \mathbf{U} . DEIM interprets that the elementwise function \mathbf{f} can be approximated as a linear combination with basis \mathbf{U} and the elements $\mathbf{c}[k]$ as function coefficients.

After obtaining \mathbf{U} from \mathbf{U}_{svd} , we then obtain \mathbf{P} with the following procedure [13]:

1. The index and value of the largest element of the first left-singular vector is stored in a list. \mathbf{P} starts as a column matrix with the only non-zero element being the value 1 at the row corresponding to this index.
2. For each column $l \geq 2$ of the POD left-singular vectors (where $\tilde{\mathbf{U}}_l$ is a matrix with the first $l - 1$ columns of \mathbf{U}):
 - (a) find \mathbf{c} where $(\mathbf{P}^T \tilde{\mathbf{U}}_l) \mathbf{c} = \mathbf{P}^T \mathbf{u}_l$, where \mathbf{u}_l is the left-singular vector corresponding to the l^{th} column of \mathbf{U} .
 - (b) Calculate $\mathbf{r} = \mathbf{u}_l - \tilde{\mathbf{U}}_l \mathbf{c}$ and store the maximum absolute value and index of \mathbf{r} in a list. Add a new column to \mathbf{P} according to the obtained index.
3. Output: Pivoting matrix \mathbf{P} according to the order dictated by the index list obtained.

This procedure guarantees that $\mathbf{P}^T \tilde{\mathbf{U}}_l$ is always nonsingular, thus \mathbf{c} is the unique solution to the linear system in step 2 [13]. Letting \mathbf{U} be the matrix of left singular values obtained from the procedure, it follows from (11) that:

$$\mathbf{c}[k] = (\mathbf{P}^T \mathbf{U})^{-1} \mathbf{P}^T \mathbf{f}(\mathbf{Tz}[k]) \quad (12)$$

This leads to a reduced-order model with DEIM:

$$\hat{\mathbf{f}}(\mathbf{Tz}[k]) \approx \mathbf{U}(\mathbf{P}^T \mathbf{U})^{-1} \mathbf{P}^T \mathbf{f}(\mathbf{Tz}[k]) \quad (13)$$

This approximation has an ℓ_2 error bound of the following form [13]:

$$e_{\ell_2}(\mathbf{f}) \leq \|(\mathbf{P}^T \mathbf{U})\|_2 \|(\mathbf{I} - \mathbf{U} \mathbf{U}^T) \mathbf{f}(\mathbf{Tz}[k])\| \quad (14)$$

where, in turn:

$$\|(\mathbf{P}^T \mathbf{U})\|_2 \leq (1 + \sqrt{2n})^{m-1} \|\mathbf{u}_1\|_\infty^{-1} \quad (15)$$

with \mathbf{u}_1 being the first column of \mathbf{U} and n being the number of original states.

The main advantage of DEIM is that, as \mathbf{f} is an element-wise nonlinear function, the following equality holds:

$$\underbrace{\mathbf{U}(\mathbf{P}^T \mathbf{U})^{-1} \mathbf{P}^T}_{\mathbf{T}_1 \in \mathbb{R}^{n \times n}} \underbrace{\mathbf{f}(\mathbf{Tz}[k])}_{\mathbf{f}: \mathbb{R}^n \rightarrow \mathbb{R}^n} = \underbrace{\mathbf{U}(\mathbf{P}^T \mathbf{U})^{-1}}_{\mathbf{T}_2 \in \mathbb{R}^{n \times m}} \underbrace{\mathbf{f}(\mathbf{P}^T \mathbf{Tz}[k])}_{\mathbf{f}: \mathbb{R}^m \rightarrow \mathbb{R}^m} \quad (16)$$

The difference between the right-hand side and left-hand side of this equation is better seen in a compact form,

$$\mathbf{T}_1 \mathbf{f}(\mathbf{Tz}[k]) = \mathbf{T}_2 \mathbf{f}(\mathbf{P}^T \mathbf{Tz}[k])$$

where \mathbf{T}_1 has n columns, which yields the same computation problem as the original Galerkin projection, whereas \mathbf{T}_2 has m columns, which is the reduced state space. This simple difference grants huge computational savings, since the online calculations would be performed in terms of the reduced dimension m , $m \ll n$, which mitigates the computation issues regarding the POD method.

The DEIM-approximated reduced order ESN has the form, obtained by applying DEIM from Eq. (16) into the already reduced ESN at (8):

$$\begin{aligned} \mathbf{z}[k+1] &= (1 - \gamma)\mathbf{z}[k] \\ &+ \gamma \mathbf{T}^T \mathbf{T}_2 \mathbf{f}(\mathbf{P}^T \mathbf{W}_r^r \mathbf{Tz}[k] + \mathbf{P}^T \mathbf{W}_i^r \mathbf{u}[k] + \mathbf{P}^T \mathbf{W}_b^r) \end{aligned} \quad (17a)$$

$$\mathbf{y}[k+1] = \mathbf{W}_r^o \mathbf{Tz}[k+1], \quad (17b)$$

The property $\mathbf{P}^T \mathbf{f}(\cdot) = \mathbf{f}(\mathbf{P}^T \cdot)$ holds for elementwise operations, which justify the matrix placement in the DEIM reduced-order ESN.

4.3. Stability Loss in DEIM

According to [31], a contractive linear system is guaranteed to retain stability when applying POD for model order reduction, therefore, if the ESN is contractive, the POD-ESN is guaranteed to retain stability. However, DEIM has no such a property. Assume an equilibrium point \mathbf{x}_{eq} of the ESN, and a fixed input \mathbf{u} ,

$$\mathbf{x}_{\text{eq}} = \mathbf{f}(\mathbf{W}_r^r \mathbf{x}_{\text{eq}} + \mathbf{W}_i^r \mathbf{u} + \mathbf{W}_b^r) \quad (18)$$

and its reduced mapping $\mathbf{z}_{\text{eq}} = \mathbf{T}^T \mathbf{x}_{\text{eq}}$. The Jacobian of the full and reduced order model are:

$$J(\mathbf{x}_{\text{eq}}) = (1 - \gamma)\mathbf{I} + \gamma \mathbf{f}'(\mathbf{g}(\mathbf{x}_{\text{eq}})) \mathbf{W}_r^r \quad (19)$$

$$J(\mathbf{z}_{\text{eq}}) = (1 - \gamma)\mathbf{I} + \gamma \mathbf{T}^T \mathbf{f}'(\mathbf{g}(\mathbf{Tz}_{\text{eq}})) \mathbf{W}_r^r \mathbf{T} \quad (20)$$

where:

$$\mathbf{g}(\mathbf{x}) = \mathbf{W}_r^r \mathbf{x} + \mathbf{W}_i^r \mathbf{u} + \mathbf{W}_b^r \quad (21)$$

Since \mathbf{f}' is a diagonal matrix where each element belongs to the interval $(0, 1]$ for being the elementwise derivative of the tanh function, the stability of the ESN in both cases is governed by \mathbf{W}_r^r at any equilibrium point. Also, as per [31], the stability of the ESN is preserved in the POD reduction. Summing up, the original and reduced-order ESNs are stable provided that the spectral radius of \mathbf{W}_r^r is smaller than 1.

With DEIM, however, the stability is not retained. This can be shown by calculating the Jacobian of an ESN reduced by both POD and DEIM:

$$\mathbf{J}_{\text{DEIM}}(\mathbf{z}) = (1 - \gamma)\mathbf{I} + \gamma\mathbf{T}^T\mathbf{U}(\mathbf{P}^T\mathbf{U})^{-1}\mathbf{f}'(\mathbf{P}^T\mathbf{g}(\mathbf{Tz}))\mathbf{P}^T\mathbf{W}_r^r\mathbf{T} \quad (22)$$

Notice that the term $(\mathbf{P}^T\mathbf{U})^{-1}$ can actually amplify the Jacobian to the point that the ESN dynamic system has an unstable eigenvalue, despite POD-ESN being stable. This term represents the pivoting of the truncated singular vectors associated with DEIM.

5. Applications

This section presents results from experiments carried out with reduced-order ESNs for three case studies.

5.1. Preliminary Study: Energy contribution distribution in Echo State Networks

POD and DEIM both originate from applying SVD into the ESN state response matrix, which in turn is obtained from exciting the ESN's reservoir with an input signal. Thus, the SVD does not depend on the output layer. To test the influence of input signals into the singular values of the state snapshots, we initialize 20 different single-input ESN reservoirs and apply SVD into the snapshots of the response obtained from the reservoir, given as inputs with 10,000 timesteps:

- A white noise following the normal distribution $\mathcal{N}(0, 1)$.
- Four different APRBS (Amplitude-modulated Pseudo-Random Binary Signal) random stair signals, defined by their minimum period, i.e., 10 timesteps, 100 timesteps, 500 timesteps, and 1,000 timesteps.
- A concatenation in time of all the signals above.

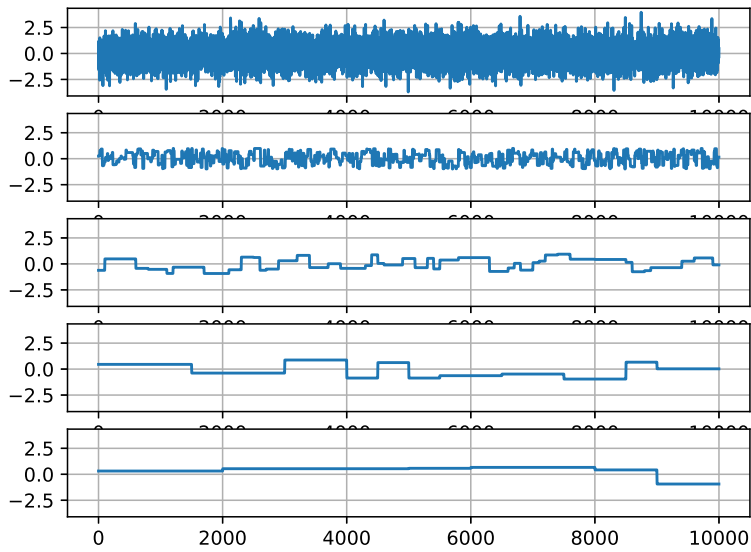


Figure 2: One-dimensional input signals for the reservoir energy contribution distribution experiment. White noise (top), APRBS signals (usually used in identification tasks): with minimum period of 10, 100, 500, and 1,000 timesteps, respectively, from second topmost plot to bottom.

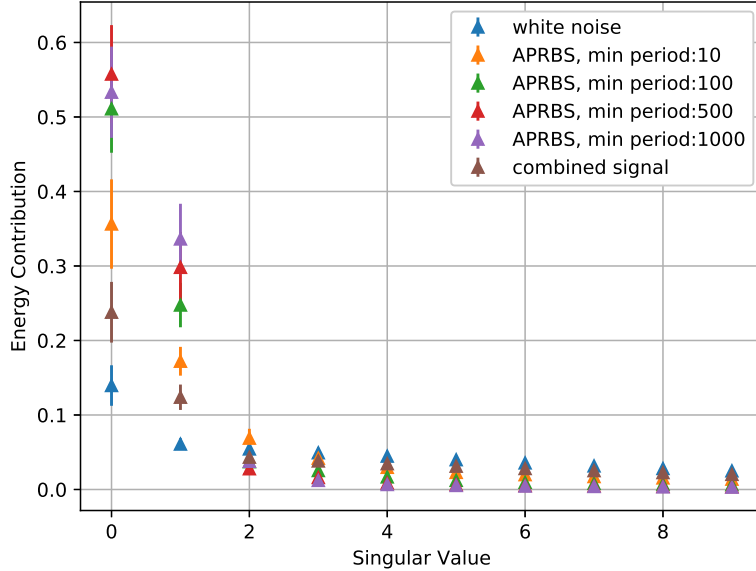


Figure 3: Mean and Standard deviation of the first ordered 10 singular values (with 0 corresponding to the highest, and 9 to lowest) obtained from the snapshots of 20 different ESN reservoirs. Each color corresponds to a different input signal fed to the ESN reservoir, shown in Fig. 2.

The input signals for the experiments are shown in Figure 2. Note that this discussion concerns only the state dynamics of the reservoir, therefore it is neither dependent on a system to be identified, nor on the output weights.

After exciting the ESN with the aforementioned signals, one at a time, we perform SVD of the resulting ESN state response snapshots and plot the energy contribution ϵ_j associated with each singular value, sorted from highest to lowest according to Eq. (7). All the reservoirs employed for this experiment are fully leaked ($\gamma = 1$), have 500 neurons, a spectral radius $\rho = 0.99$, and a value 0.1 for both input scaling and bias scaling.

Figure 3 showcases the mean and standard deviation of the energy contribution of the 10 highest singular values for each state snapshot considering 20 randomly initialized reservoirs. We infer from this result that the singular values are more evenly distributed the higher the frequencies of the input signal are. As the white noise is a signal with heavy high frequency information, the ESN state response is expected to have a more even energy

contribution distribution among the singular values.

Meanwhile, the lower frequency signals have the energy contribution concentrated about the highest magnitude singular value. In fact, real-life dynamic systems work as low pass filters [29] and, therefore, they are expected to have lower frequency information. The slower the dynamics of a system are, the larger the minimum period of an APRBS signal needs to be, which directly affects the singular value profile of the model order reduction.

The implication of this experiment is that, since the distribution of the energy contribution depends entirely on the input signal frequency, the number of states that can be pruned for MOR is higher for cases with low frequency dynamics. As an easy example, the highest energy contribution singular value for APRBS signal with minimum period of 1,000 timesteps contributes more to the total energy of the snapshots than the sum of the 10 highest singular values for the white noise shown in the plot.

5.2. Memory Capacity Evaluation

Short-term Memory Capacity (MC) is a well known metric for Echo State Networks [15] that measures how well an ESN can remember past inputs and general dynamic storage capacity. MC serves as a performance measurement for a given ESN reservoir, which is obtained from the following procedure:

- For an arbitrary n , train a single-input, single-output Echo State Network so that the input is a given white noise $\eta[k]$, and the output is the same white noise delayed n timesteps $\eta[k - n]$. In layman’s terms, the ESN is supposed to “memorize” the input from n timesteps ago.
- Obtain the correlation coefficient R_n for the training with an arbitrary n ,

$$R_n = \frac{\text{cov}(y_{esn}, \eta[k - n])}{\text{var}(\mathbf{y}_{esn})\text{var}(\eta[k - n])} \quad (23)$$

where $\text{cov}(\cdot)$ is the covariance operator, y_{esn} is the single ESN output, $\text{var}(\cdot)$ is the variance operator, and, therefore, R_n is merely the determination coefficient for a given delay n .

- The memory capacity is calculated, in theory, as:

$$MC = \sum_{n=1}^{\infty} R_n \quad (24)$$

The MC of an ESN was mathematically proven to have an upper bound in its number of neurons N [15], which means that it is directly related to the number of network neurons.

For this work, we propose an experiment to compare the memory capacity of the reduced order model of the ESN, and the original ESN, as the number of neurons is directly tied to the upper bound. Since it is impossible to make infinite training experiments, we define the memory capacity for this experiment as follows:

$$MC = \sum_{n=1}^{N_{MC}} R_n \quad (25)$$

where $N_{MC} = 100$ is a large enough number to measure the memory capacity of the network. As preliminary tests show, after a given n , the determination coefficient converges to a low value. Therefore, the information regarding memory capacity is more concentrated in the lower n spectrum, endorsing the limited number of experiments ($N_{MC} = 100$) for comparison purposes.

5.2.1. POD reduction

We ran the memory capacity experiment for different numbers of neurons ($N = \{400, 600, 800, 1000, 1200, 1400, 1600, 1800, 2000, 2200\}$) with an Energy Cutoff (EC) of 1%, 5%, and 10%. Since the reservoir of an ESN is initialized at random, we perform model order reduction for 12 different reservoirs in each configuration. We then measure the mean and standard deviation for the memory capacity of these 12 runs, while also obtaining the range of the reduced dimension for a given energy cutoff. This allows us to measure not only the memory capacity drop for the model order reduction, but also how reservoir-dependent the reduction procedure is.

All reservoirs analyzed are fully leaked ($\gamma = 1.0$), and have input and bias scaling at 0.1. Also, the reservoir spectral radius is $\rho = 0.99$.

Figure 4 showcases the results of the Memory Capacity experiments when performing MOR at the tested ESNs given different energy cutoffs, depicting both mean and standard deviation of the 12 runs.

The first plot is depicted in terms of the number of ESN neurons before applying POD to a given network. It shows the expected drop in MC as MOR is performed with more energy cutoff.

Meanwhile, the second plot portrays the MC as a function of the exact number of states of a given network after performing MOR through POD.

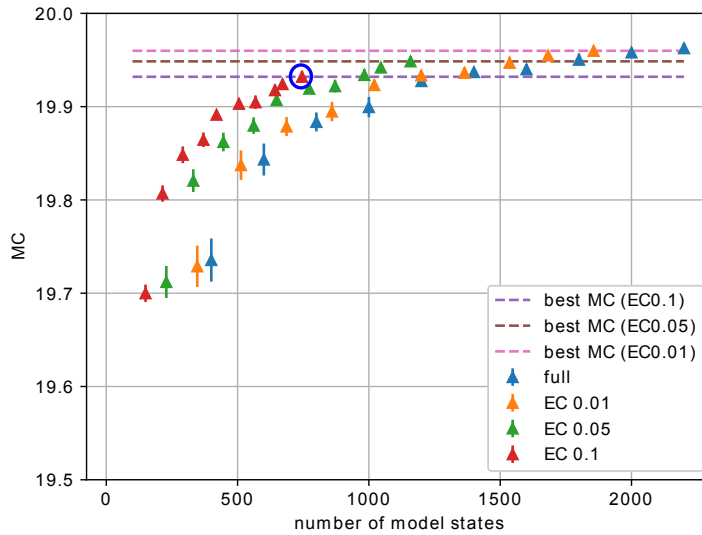
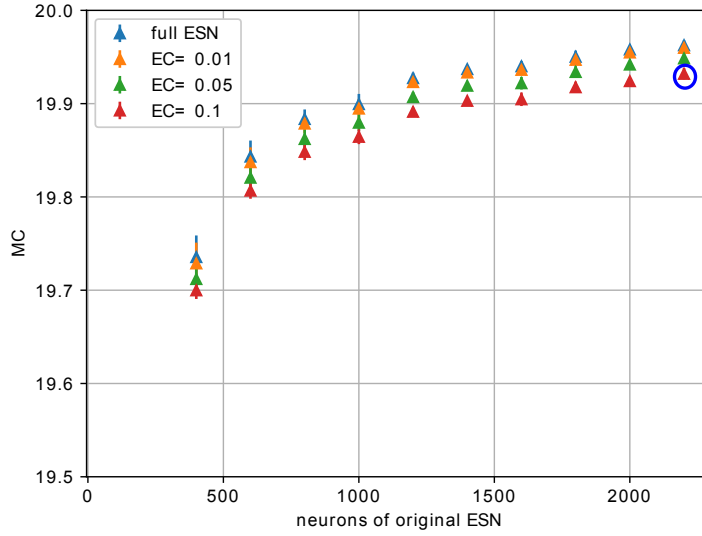


Figure 4: Plot of the memory capacity as a function of the number of neurons of the original network (upper plot), and as a function of the number of states (lower plot). Each point is colored according to the energy cutoff of the POD-ESN that obtained the MC shown (points in blue are the MC obtained from full ESNs). EC means the energy cutoff of the applied POD.

As MC progresses monotonically given the number of states, either in an ESN or in a given MOR of that ESN, it becomes easy to map a point of the second plot into the first one: for example, the last red point (from left to right) of both plots (marked within a blue circle) have the same memory capacity since they correspond to the same network/EC configuration. Thus, the MOR of an ESN with 2200 neurons (first plot) has roughly 750 states (second plot) at 1% energy cutoff.

As per the previous section, since a white noise signal is traditionally employed for this experiment, the drop in the number of reduced states is not very significant, however the drop in MC is still small given that a large number of states were still cut off (even in the case of 10% energy cutoff for the 2200 neurons case, the number of states was reduced to almost a third). In fact, the second plot shows that a POD-reduced network ends up being more powerful in terms of MC than a full (non-reduced) ESN with the same number of states. Of course, the better performance is justifiable in that a POD-reduced ESN is still more structurally complex than a smaller ESN with the same number of neurons.

5.2.2. DEIM reduction

We also performed DEIM for each POD-ESN obtained, to further reduce the number of tanh in the computations and evaluate the drop in MC in comparison to the POD-reduced ESN. We tested four different energy cutoff configurations for the DEIM: {1%, 5%, 10%, 20%}. Table 1 shows the results of applying these DEIM configurations into each POD for three original reservoir sizes $N = \{800, 1400, 2000\}$ (from topmost table to the bottom-most one, respectively). It presents the results for the DEIM reduction, where the memory capacity is evaluated for each configuration in energy cutoff for both POD and DEIM. The number in parenthesis is the actual dimension resulting from the reduction. Each column corresponds to a different energy cutoff configuration for DEIM, evaluated in the first row, while each row represents a different energy cutoff configuration for POD, evaluated in the first column. For instance, the MC of an ESN with a 1% energy cutoff POD (yielding 1,119 states when $N = 1,400$) and a 5% energy cutoff DEIM (yielding 748 tanh function evaluations when $N = 1,400$) is 0.099, 0.03 and 0.02 for $N = 800, 1400, 2000$ respectively. Notice that there was no POD reduction for the first row of each table, as well as no DEIM reduction for the first column of each table. The empty cells refer to the fact that DEIM can not be employed without first applying the POD reduction.

Table 1: Memory capacity evaluated for different energy cutoffs used in POD and DEIM. Each table considers an original ESN of different size N , to be reduced.

$N = 800$	Energy Cutoff (EC) for DEIM				
EC (POD)	0%	1%(678)	5%(430)	10%(279)	20%(128)
0%(800)	19.88 ± 0.01	–	–	–	–
1%(686)	19.87 ± 0.01	0.44 ± 0.20	0.099 ± 0.01	0.08 ± 0.04	0.54 ± 0.18
5%(445)	19.86 ± 0.01	16.48 ± 2.21	0.059 ± 0.026	0.096 ± 0.02	0.55 ± 0.17
10%(291)	19.84 ± 0.008	19.68 ± 0.03	0.99 ± 0.25	0.097 ± 0.02	0.54 ± 0.18

$N = 1,400$	Energy Cutoff (EC) for DEIM				
EC (POD)	0%	1%(1,186)	5%(748)	10%(484)	20%(226)
0%(1,400)	19.93 ± 0.003	–	–	–	–
1%(1,119)	19.93 ± 0.003	0.11 ± 0.03	0.03 ± 0.03	0.04 ± 0.02	0.17 ± 0.05
5%(772)	19.91 ± 0.003	3.189 ± 1.09	0.03 ± 0.02	0.04 ± 0.02	0.17 ± 0.04
10%(505)	19.90 ± 0.003	19.18 ± 0.50	0.19 ± 0.02	0.025 ± 0.02	0.17 ± 0.05

$N = 2,000$	Energy Cutoff (EC) for DEIM				
EC (POD)	0%	1%(1,835)	5%(1,122)	10%(713)	20%(333)
0%(2,000)	19.96 ± 0.002	–	–	–	–
1%(1,682)	19.95 ± 0.002	0.06 ± 0.01	0.02 ± 0.02	0.03 ± 0.01	0.03 ± 0.03
5%(1,045)	19.94 ± 0.002	1.2 ± 0.4	0.01 ± 0.02	0.02 ± 0.02	0.08 ± 0.03
10%(671)	19.92 ± 0.002	18.37 ± 0.90	0.09 ± 0.03	0.04 ± 0.01	0.07 ± 0.03

The only time DEIM managed to actually represent relatively well the MOR was when there was an 1% energy cutoff for DEIM considering 10% energy cutoff for POD. That is, DEIM is actually being performed for smaller reduced order models. In general, performance is mildly better whenever DEIM has a higher number of states ratio in comparison to the POD states. For this experiment, DEIM was not expected to perform well, as the white noise signal does not allow for a great reduction of states, as it is a highly heavy information signal.

5.3. NARMA System

As an initial case study for the POD reduction of the ESN, we try to identify the behavior of a so-called NARMA (Nonlinear Autoregressive Moving Average) difference equation system [16], equated as follows:

$$y[k] = 0.3y[k - 1] + 0.05y[k - 1] \sum_{i=1}^m y[k - i] + 1.5u[k - m + 1]u[k] + 0.1 \quad (26)$$

where $m = 10$ is the order of the system.

As in [16], the excitation signal applied in (26) is drawn from the random uniform distribution with value range of $0 \leq u[k] \leq 0.05$. A simulation of 5,000 time steps is performed where the first 2,000 samples are labeled as training data and the rest is labeled as test data. In this work, the R^2 metric is employed to measure network performance.

With the aforementioned dataset, we train an ESN with the following configuration: 1,400 neurons in the reservoir layer, high enough so that we show the MOR potential at work; a leak rate of $\gamma = 0.7$; scaling of 0.1 for both bias and input connections; and spectral radius of $\rho = 0.99$. In terms of R^2 , the network had a performance of 0.95949337 for the NARMA model output. We will now carry out experiments of POD for this network to evaluate how the MOR performs in terms of R^2 in relation to the original 1,400 units network. Figure 5 showcases the experiment with POD reduction being performed so that the ESN is reduced to the number of states in the x axis (blue dots). For comparison, we also plotted the R^2 for the exact same NARMA experiment with 10 runs of full (non-reduced) ESNs which have the same reservoir size as the networks that underwent POD reduction (orange triangles). The POD-ESN reduction generally achieved superior performance

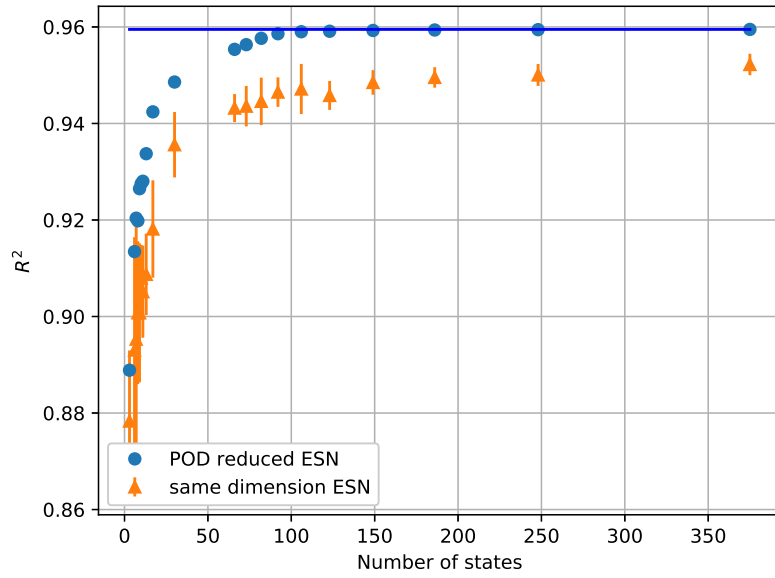


Figure 5: Experiment comparing a POD-reduced ESN (blue dots) with a ESN of equivalent size (to the reduced ESN) (orange triangles) for the 10th order NARMA task. The POD reduction is applied on a ESN with 1,400 units in the reservoir. The horizontal axis is the number of states (units) of the reduced (full) network, while the vertical axis is the R^2 metric on test set. The R^2 of the 1,400 units ESN is also plotted as a blue horizontal line for comparison.

over the full ESN at the same reservoir size, which is understandable, as the POD-ESN is not only supposed to be an emulation of a larger ESN behavior, but is also more complex in structure. The NARMA experiment also show that the R^2 metric for ESNs reduced to at least 50 states is very similar to the metric achieved by the original 1,400 units ESN, i.e., the blue dots are very close to the horizontal blue line in the plot of Figure 5 when the number of states is higher than 50.

5.4. Two Wells and One Riser Platform

We now test the MOR over the ESN for a physical problem: an oil production platform consisting of two gas-lifted oil wells and one riser, as illustrated in Figure 6. To gather data, we utilize a composite model between two well models, a riser model, and a manifold that serves as a connector to the three units. All models assume a 2-phase fluid containing gas and liquid. The well model assumes two control volumes in the gas injection annulus and the production tubing, with boundary conditions for: gas-lift pressure, reservoir pressure, and outlet pressure. The riser model considers a horizontal pipeline and the vertical portion of the riser as two separate control volumes, and assumes the inlet flow, and outlet pressure as boundary conditions. The manifold assumes no load loss due to friction, therefore it equates each well output flow to the riser input flow, and the riser inlet pressure. Overall, the whole system has 120 algebraic variables, 10 state variables, 5 input variables, and exactly 5 boundary conditions. The well is modeled as described with more details in [32], while the riser model is described in [33]. The model configuration is exactly the same as the one described in [34]. The reader can refer to these works for more details on the mathematical modeling of the platform.

The experiment with the two-well production platform is used to depict how to achieve MOR with ESNs from a system identification standpoint. First, we must train an ESN model for the two-well and one-riser platform. We generate 50,000 timesteps of data from numerical simulation of the platform model, yielding a dataset where the 2-dimensional input to the ESN is composed of both well production chokes $u_{ch,1}$ and $u_{ch,2}$, while the desired 2-dimensional output of the network corresponds to each well bottom-hole pressure: $P_{bh,1}$, $P_{bh,2}$. The training dataset consist of the first 10,000 timesteps, while the segment from $k = 20,000$ to $k = 30,000$ is used as a validation set, and the rest ($k > 30,000$) as a test set. With the described dataset, we train an ESN with 1,400 reservoir units (chosen this high for the sake of

demonstrating the MOR potential at work), a leak rate of $\gamma = 0.7$, scalings for both bias and input equal to 0.1, and spectral radius $\rho = 0.99$. In terms of R^2 metric, the network had a test performance of (0.99881673, 0.99900379) for each individual well bottom-hole pressure.

Now, we will run POD experiments with the previously trained network to assess how MOR performs in terms of R^2 in relation to the original 1,400 units network. Figure 7 depicts an experiment where MOR of different state sizes were tested in terms of R^2 over the test data. One can infer that after a given number of states (150) the performance remains consistently close to the original network in terms of R^2 , despite having only 10% of the original number of states.

PODs that resulted in 92 states also showcased good performance in comparison to the original network of 1,400 neurons. However, with only POD, the computational problem of computing $\mathbf{T}^T \mathbf{f}$ still remains. We select the case where the reduced network has 92 states (which represents an energy

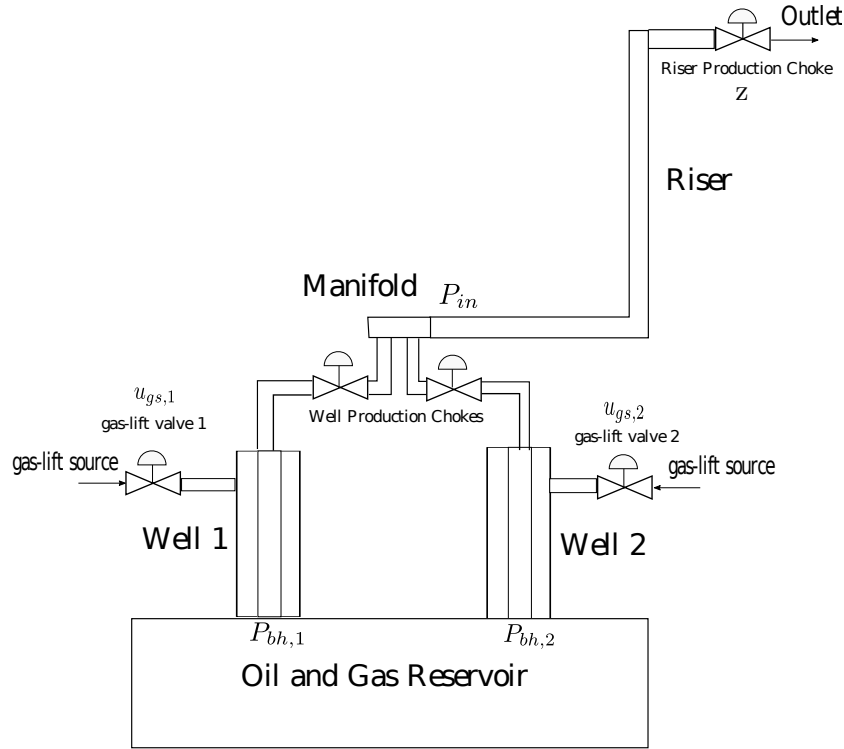


Figure 6: Representation of an oil platform containing two wells and one riser. From [17].

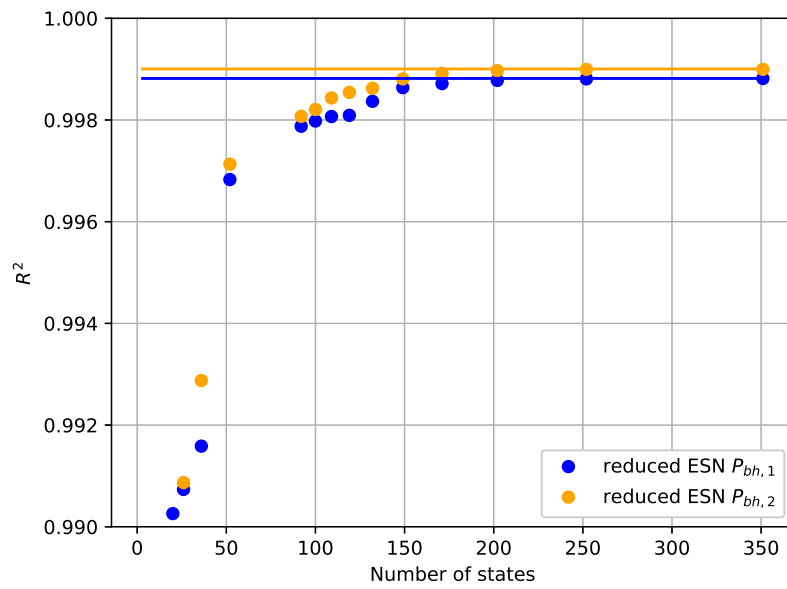


Figure 7: POD-ESN for a system identification task. The full ESN network has 1,400 neurons, which was trained to model the platform with two wells and one riser. The x axis is the number of states of the reduced network, whereas the y axis is the R^2 metric on the test set for each individual output variable (bottomhole pressures). The bottom-hole pressure of the first well is represented in blue color, while the orange color denotes the bottom-hole pressure of the second well. The R^2 of the original network is also plotted as horizontal lines of corresponding colors for comparison.

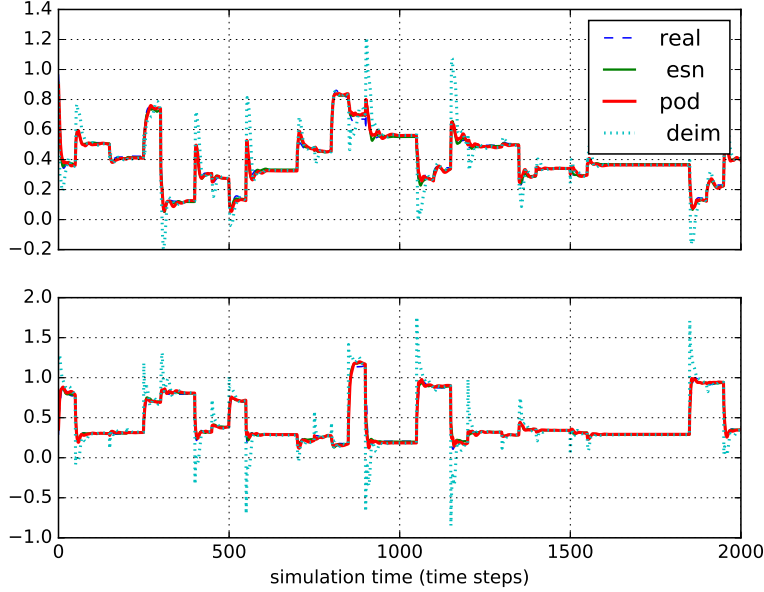


Figure 8: Single simulation run involving a POD with 92 states (0.01 energy cutoff) and a DEIM interpolation with $m = 1,073$, put side by side with the original data for the bottom hole pressure p_{bh} of both wells (normalized), and the original ESN.

cutoff of 1%), and try performing DEIM on it. Figure 8 depicts a simulation for the ESN, POD-ESN, and POD-DEIM ESN for the test data of the two-wells and one riser platform. Even though there was a reduction from 1,400 to only 92 states, the behavior of the ESN and the POD-ESN managed to be close in terms of dynamics. With the application of DEIM, the computation nodes were reduced from 1,400 to 1,073, however some overshooting emerged which was not present in the ESN and POD-ESN. With respect to the simulation run in Figure 8, the R^2 for each well normalized bottom-hole pressure was: (0.9988, 0.9990) for the ESN, (0.9979, 0.9981) for the POD-ESN, and (0.9873, 0.9671) for the DEIM-POD-ESN. There is little drop in response quality from reducing the number of states from 1,400 to 92 through POD, but performing interpolation from a standard POD to a POD-DEIM framework seems to affect the response more significantly.

6. Discussion

POD showed a response close to the original ESN for both the NARMA and the two wells/one riser case studies, and a very minor loss in MC during the reduction. However, this was not shown to be the case when DEIM was applied. There seems to be more loss of dynamic information when DEIM is performed than when POD is, as POD retains the number of activation functions being computed even though the number of states is diminished. Thus, we conjecture that the capacity of a reservoir to represent accurately a nonlinear system is more influenced by the combination of the nonlinear functions in a high-dimensional space (in the context of MOR, given by the projection of the reduced states back to the original space, just before applying the tanh nonlinearity) than maintaining a high-dimensionality of the reservoir states themselves.

In terms of memory, however, there is some reduction resulting from the application of POD. First, the state-to-output linear combination matrix $\mathbf{W}_r^o \mathbf{T}$ diminishes in size and maps the reduced space directly to the output. Also, the computation of the activation function becomes slightly less expensive memory-wise because of the term $\mathbf{W}_r^r \mathbf{T}$, as this offline-computed product results in a matrix with less elements overall. Of course, the resulting matrix is still larger in comparison to an ESN with the same size as the reduction, which makes the same-size ESN less complex than the POD-reduced one.

Even though POD computes the same number of activation functions as the original ESN, the computation time is significantly reduced, as shown in Table 2. This table shows the mean time it took to execute a step in the full ESN against the time it took to execute a POD-ESN computation step, for the NARMA experiment. For instance, when applying POD-ESN to reduce from 1400 states to 66 states, we get an 80% decrease in mean execution time (from 0.767 ms to 0.147 ms), while still maintaining a very good performance, as this setup is near the horizontal line in Figure 5. All experiments were performed under similar conditions, with the same computer.

As shown in Table 2, even though there is no computation reduction in the nonlinear nodes, the computational time for a POD-ESN to compute a time step is actually diminished, even if by a small margin.

The loss of stability incurred in ESNs by DEIM, as previously discussed, was corroborated by their poor performance achieved in the Memory Capacity experiments. Besides, even when the DEIM-reduced ESN dynamic system remained stable, as in the two-well experiment illustrated in Figure

Table 2: Mean execution time for the NARMA experiment composed of 5,000 time steps.

	Mean Execution Time (ms)	St. Dev. (ms)
ESN (size=1400)	0.767	0.537
POD (size=3)	0.072	0.0498
POD (size=6)	0.078	0.0251
POD (size=7)	0.141	0.391
POD (size=8)	0.131	0.340
POD (size=9)	0.160	0.543
POD (size=10)	0.140	0.467
POD (size=11)	0.233	0.955
POD (size=13)	0.105	0.122
POD (size=17)	0.106	0.0738
POD (size=30)	0.135	0.0856
POD (size=66)	0.147	0.254
POD (size=73)	0.144	0.138
POD (size=82)	0.141	0.140
POD (size=92)	0.155	0.109
POD (size=106)	0.151	0.0744
POD (size=123)	0.149	0.0907
POD (size=149)	0.183	0.407
POD (size=186)	0.201	0.145
POD (size=248)	0.230	0.134
POD (size=375)	0.408	0.199

8, the system experienced high overshoots which translates into modeling error. The independent work [35] that also implements POD/DEIM on ESN, which appeared in the literature during the writing of this research, proposes a method to deal with the stability issue. However, the method is restricted to the special class of ESNs with dynamic equations without the bias term. That method relies on expanding the nonlinear dynamics reduced by the DEIM, so that the Jacobian contribution of the terms affected by $(\mathbf{P}^T \mathbf{U})$ becomes null with respect to $\mathbf{u} = \mathbf{0}$. In this context, generalized methods (that take into account the bias term as well) to guarantee stability retention of an ESN interpolated by DEIM are an interesting topic for future works.

7. Conclusion

In this investigation, the POD was shown to achieve exceptional results in terms of reducing the number of states of an ESN and maintaining performance. The reduced ESN managed to perform almost as well as the original ESN, despite the the drastic reduction of states in a normal system identification task. This work also showcased how the nature of the excitation signal changes the singular value profile of the SVD, concluding that more efficient reductions can be performed for lower frequency input signals. This is to say that, ideally, the excitation signal for a system to be identified should be as slow as necessary. In addition, the memory capacity test was performed with signals that carry information from all frequencies, and even then the reduced network showcased better performance than an ESN of the same size trained on the data. This happens arguably because the POD-reduced ESN emulates the behavior of the larger original ESN from which it was reduced, and also for its more complex structure when compared to a same size ESN.

Acknowledgements

Funding: This work was supported by Coordenação de Aperfeiçoamento de Pessoal de Nível Superior (CAPES); and Fundação de Amparo à Pesquisa e Inovação do Estado de Santa Catarina (FAPESC) [grant number 2021TR2265].

References

- [1] O. Nelles, *Nonlinear System Identification: From Classical Approaches to Neural Networks and Fuzzy Models*, 1 ed., Springer, Berlin, 2001.
- [2] C. M. Bishop, *Pattern Recognition and Machine Learning (Information Science and Statistics)*, Springer-Verlag Inc., New York, 2006.
- [3] I. Goodfellow, Y. Bengio, A. Courville, *Deep Learning*, MIT Press, 2016. <http://www.deeplearningbook.org>.
- [4] M. C. Mozer, A focused backpropagation algorithm for temporal pattern recognition, *Complex Systems* 3 (1989) 349–381.
- [5] S. Hochreiter, J. Schmidhuber, Long short-term memory, *Neural Computation* 9 (1997) 1735–80. doi:10.1162/neco.1997.9.8.1735.

- [6] H. Jaeger, M. Lukosevicius, D. Popovici, U. Siewert, Optimization and applications of echo state networks with leaky-integrator neurons, *Neural Networks* 20 (2007) 335–352. doi:10.1016/j.neunet.2007.04.016.
- [7] W. Maass, Liquid state machines: Motivation, theory, and applications, in: *Computability in Context*, Imperial College Press, 2011, pp. 275–296. URL: https://doi.org/10.1142/9781848162778_0008. doi:10.1142/9781848162778_0008.
- [8] E. A. Antonelo, B. Schrauwen, On learning navigation behaviors for small mobile robots with reservoir computing architectures, *IEEE Transactions on Neural Networks and Learning Systems* 26 (2015) 763–780.
- [9] R. Mezzi, N. Yousfi-Steiner, M. C. Péra, D. Hissel, L. Larger, An echo state network for fuel cell lifetime prediction under a dynamic micro-generation load profile, *Applied Energy* 283 (2021) 116297. URL: <https://www.sciencedirect.com/science/article/pii/S0306261920316834>. doi:<https://doi.org/10.1016/j.apenergy.2020.116297>.
- [10] Y. Bai, M.-D. Liu, L. Ding, Y.-J. Ma, Double-layer staged training echo-state networks for wind speed prediction using variational mode decomposition, *Applied Energy* 301 (2021) 117461. URL: <https://www.sciencedirect.com/science/article/pii/S0306261921008503>. doi:<https://doi.org/10.1016/j.apenergy.2021.117461>.
- [11] S. F. Stefenon, L. O. Seman, N. F. Sopelsa Neto, L. H. Meyer, A. Nied, K.-C. Yow, Echo state network applied for classification of medium voltage insulators, *International Journal of Electrical Power & Energy Systems* 134 (2022) 107336. URL: <https://www.sciencedirect.com/science/article/pii/S0142061521005755>. doi:<https://doi.org/10.1016/j.ijepes.2021.107336>.
- [12] E. Camacho, C. Bordons, *Model Predictive Control*, Springer, 1999.
- [13] S. Chaturantabut, D. C. Sorensen, Nonlinear model reduction via discrete empirical interpolation, *SIAM Journal on Scientific Computing* 32 (2010) 2737–2764. URL: <https://doi.org/10.1137/090766498>. doi:10.1137/090766498.
- [14] Y. Wang, B. Yu, Y. Wang, Acceleration of gas reservoir simulation using proper orthogonal decomposition, *Geofluids*

- 2018 (2018) 1–15. URL: <https://doi.org/10.1155/2018/8482352>. doi:10.1155/2018/8482352.
- [15] H. Jaeger, Short term memory in echo state networks, Technical Report GMD Report 152, German National Research Center for Information Technology, 2002.
- [16] Y. Sakemi, K. Morino, T. Leleu, K. Aihara, Model-size reduction for reservoir computing by concatenating internal states through time, *Scientific Reports* 10 (2020). doi:10.1038/s41598-020-78725-0.
- [17] J. P. Jordanou, E. A. Antonelo, E. Camponogara, Online learning control with echo state networks of an oil production platform, *Eng. Appl. Artif. Intell.* 85 (2019) 214–228. doi:<https://doi.org/10.1016/j.engappai.2019.06.011>.
- [18] B. Whiteaker, P. Gerstoft, Reducing echo state network size with controllability matrices, *Chaos: An Interdisciplinary Journal of Nonlinear Science* 32 (2022) 073116. URL: <https://doi.org/10.1063/5.0071926>. doi:10.1063/5.0071926.
- [19] W. Liu, Y. Bai, X. Jin, X. Wang, T. Su, J. Kong, Broad echo state network with reservoir pruning for nonstationary time series prediction, *Computational Intelligence and Neuroscience* 2022 (2022) 1–15. URL: <https://doi.org/10.1155/2022/3672905>. doi:10.1155/2022/3672905.
- [20] C. Yang, Z. Wu, Multi-objective sparse echo state network, *Neural Computing and Applications* (2022). URL: <https://doi.org/10.1007/s00521-022-07711-6>. doi:10.1007/s00521-022-07711-6.
- [21] A. Rodan, P. Tino, Minimum complexity echo state network, *IEEE Transactions on Neural Networks* 22 (2011) 131–44. doi:10.1109/TNN.2010.2089641.
- [22] S. Løkse, F. M. Bianchi, R. Jenssen, Training echo state networks with regularization through dimensionality reduction, *Cognitive Computation* 9 (2017) 364–378. doi:10.1007/s12559-017-9450-z.

- [23] A. Haluszczynski, J. Aumeier, J. Herteux, C. R ath, Reducing network size and improving prediction stability of reservoir computing, *Chaos: An Interdisciplinary Journal of Nonlinear Science* 30 (2020) 063136. URL: <https://doi.org/10.1063/5.0006869>. doi:10.1063/5.0006869.
- [24] H. Jaeger, H. Haas, Harnessing nonlinearity: predicting chaotic systems and saving energy in wireless telecommunication, *Science* 304 (2004) 78–80.
- [25] H. Jaeger, The “echo state” approach to analysing and training recurrent neural networks – with an Erratum note, Technical Report GMD 148, Fraunhofer Institute for Autonomous Intelligent Systems, 2001.
- [26] M. C. Ozturk, D. Xu, J. C. Pr ncipe, Analysis and design of echo state networks, *Neural Computation* 19 (2007) 111–138.
- [27] D. Verstraeten, B. Schrauwen, On the quantification of dynamics in reservoir computing, in: C. Alippi, M. Polycarpou, C. Panayiotou, G. Ellinas (Eds.), *Artificial Neural Networks*, 2009, pp. 985–994.
- [28] D. Verstraeten, J. Dambre, X. Dutoit, B. Schrauwen, Memory versus non-linearity in reservoirs, in: *Int. Joint Conference on Neural Networks*, IEEE, Barcelona, Spain, 2010, pp. 18–23.
- [29] C.-T. Chen, *Linear System Theory and Design*, 3rd ed., Oxford University Press, Inc., New York, NY, USA, 1998.
- [30] X. Sun, M. Xu, Optimal control of water flooding reservoir using proper orthogonal decomposition, *Journal of Computational and Applied Mathematics* 320 (2017) 120–137. URL: <https://www.sciencedirect.com/science/article/pii/S0377042717300419>. doi:<https://doi.org/10.1016/j.cam.2017.01.020>.
- [31] R. C. Selga, B. Lohmann, R. Eid, Stability preservation in projection-based model order reduction of large scale systems, *European Journal of Control* 18 (2012) 122–132. doi:<https://doi.org/10.3166/ejc.18.122-132>.

- [32] E. Jahanshahi, S. Skogestad, H. Hansen, Control structure design for stabilizing unstable gas-lift oil wells, *IFAC Proceedings Volumes* 45 (2012) 93–100.
- [33] E. Jahanshahi, S. Skogestad, Simplified dynamical models for control of severe slugging in multiphase risers, *IFAC Proceedings Volumes* 44 (2011) 1634–1639.
- [34] J. P. Jordanou, E. A. Antonelo, E. Camponogara, Echo state networks for practical nonlinear model predictive control of unknown dynamic systems, *IEEE Transactions on Neural Networks and Learning Systems* 33 (2022) 2615–2629. doi:10.1109/TNNLS.2021.3136357.
- [35] H. Wang, X. Long, X.-X. Liu, fastesn: Fast echo state network, *IEEE Transactions on Neural Networks and Learning Systems* (2022) 1–15. doi:10.1109/TNNLS.2022.3167466.